Published in final edited form as:
Nat Microbiol. 2018 August ; 3(8): 920–931. doi:10.1038/s41564-018-0191-x.

The Type VI secretion system deploys anti-fungal effectors against microbial competitors

Katharina Trunk[1], **Julien Peltier**[2,4], **Yi-Chia Liu**[1], **Brian D. Dill**[2], **Louise Walker**[6], **Neil A.R. Gow**[6], **Michael J.R. Stark**[3], **Janet Quinn**[4], **Henrik Strahl**[5], **Matthias Trost**[2,4,*], and **Sarah J. Coulthurst**[1,*]

[1]Division of Molecular Microbiology, School of Life Sciences, University of Dundee, Dow St, Dundee, DD1 5EH, UK

[2]MRC Protein Phosphorylation and Ubiquitylation Unit, School of Life Sciences, University of Dundee, Dow St, Dundee, DD1 5EH, UK

[3]Centre for Gene Regulation and Expression, School of Life Sciences, University of Dundee, Dow St, Dundee, DD1 5EH, UK

[4]Institute for Cell and Molecular Biosciences, Newcastle University, Framlington Place, Newcastle-upon-Tyne, NE2 4HH, UK

[5]Centre for Bacterial Cell Biology, Newcastle University, Richardson Road, Newcastle-upon-Tyne, NE2 4AX, UK

[6]Aberdeen Fungal Group, Institute of Medical Sciences, MRC Centre for Medical Mycology at the University of Aberdeen, Foresterhill, Aberdeen, AB25 2ZD, UK

Abstract

Interactions between bacterial and fungal cells shape many polymicrobial communities. Bacteria elaborate diverse strategies to interact and compete with other organisms, including the deployment of protein secretion systems. The Type VI secretion system (T6SS) delivers toxic effector proteins into host eukaryotic cells and competitor bacterial cells. Yet surprisingly, T6SS-delivered effectors targeting fungal cells have not been reported. Here we show that the 'anti-bacterial' T6SS of *Serratia marcescens* can act against fungal cells, including pathogenic *Candida* species, and identify the previously-undescribed effector proteins responsible. These anti-fungal

[*]**Correspondence and requests for materials** should be addressed to Sarah Coulthurst (s.j.coulthurst@dundee.ac.uk) or Matthias Trost (matthias.trost@newcastle.ac.uk).

Data availability

Raw mass spectrometry data that support the findings of this study have been deposited to the ProteomeXchange Consortium via the PRIDE64 partner repository with the dataset identifier PXD006916. All other data supporting the findings of this study are available within the paper and its supplementary information files.

Author Contributions

K.T., M.T. and S.J.C conceived the study and designed experiments; K.T., J.P., Y.L., B.D.D., L.W. and H.S. performed experimental work, J.P. and H.S. additionally performed data analysis; J.Q., M.J.R.S and N.A.R.G. contributed expertise and reagents; K.T., M.T and S.J.C. analysed data and wrote the manuscript.

Competing Financial Interests

The authors declare no competing financial interests.

Europe PMC Funders Author Manuscripts

effectors, Tfe1 and Tfe2, have distinct impacts on the target cell, but both can ultimately cause fungal cell death. ‘In competition’ proteomics analysis revealed that T6SS-mediated delivery of Tfe2 disrupts nutrient uptake and amino acid metabolism in fungal cells, and leads to the induction of autophagy. Intoxication by Tfe1, in contrast, causes a loss of plasma membrane potential. Our findings extend the repertoire of the T6SS and suggest that anti-fungal T6SSs represent widespread and important determinants of the outcome of bacterial-fungal interactions.

Bacteria and fungi frequently cohabit in a multitude of different environments, from abiotic surroundings, such as soil, to plant and mammalian hosts, including polymicrobial infection sites. Bacteria may develop strategies to profit from the metabolic activity of neighbouring fungal cells, for example utilising fungal breakdown products from otherwise inaccessible organic material. Conversely, they may elaborate antagonistic strategies to contain growth of competing microbes, such as efficient scavenging of scarce nutrients or direct attack upon the competitor1, 2. Gram-negative bacteria utilise complex transport machineries, protein secretion systems, to translocate effector proteins into other cells3. Following translocation, the bacterial effector destroys or reprogrammes the target cell for the benefit of the secreting bacterium. The Type VI secretion system (T6SS) is a widespread, bacteriophage-like machinery that fires toxic effectors into neighbouring cells. It uses a tubular contractile sheath to expel a cell-puncturing structure, decorated with a variety of effector proteins, out of the bacterial cell towards the target 4–6. Some of these effectors are deployed against higher eukaryotes, representing classical anti-host virulence factors7. Nevertheless, recent findings indicate that the function of most T6SSs is to deliver anti-bacterial toxins into rival bacterial cells, providing a competitive advantage in mixed bacterial populations. These T6SS-delivered anti-bacterial effectors, including toxins targeting the bacterial cell wall, cell membrane and nucleic acids, are each associated with a specific immunity protein to protect the secreting cell and its siblings from self-intoxication8, 9. Surprisingly, however, given the close association of bacteria and fungi in many environments, no anti-fungal effectors delivered by the T6SS have been reported to date.

Results

The anti-bacterial T6SS of *Serratia marcescens* displays anti-fungal activity

To investigate whether the bacterial T6SS could affect proliferation of eukaryotic microorganisms commonly encountered in microbial communities, the ubiquitous yeast *Saccharomyces cerevisiae* was used as a model target organism. *Serratia marcescens* Db10, which possesses a well-characterised and potent anti-bacterial T6SS10, was utilised as the bacterial ‘attacker’. Co-culture of these two organisms resulted in >100-fold decrease of recovered viable yeast cells, indicating that *S. marcescens*, itself a ubiquitous microorganism, can restrict fungal proliferation in mixed microbial cultures (Fig. 1a). When co-cultures were performed using *S. marcescens* Δ*tssE*, a T6SS-inactive mutant, recovery of viable fungal cells was unaffected, demonstrating that the observed inhibition is T6SS-dependent (Fig. 1a). Direct translocation of effector proteins into a target cell requires the T6SS to puncture and traverse the target cell wall. Considering the thickness and rigidity of the fungal cell wall11 and that the *S. marcescens* T6SS readily releases secreted proteins to the extracellular medium12, we considered that anti-fungal toxins might instead be secreted

Europe PMC Funders Author Manuscripts

into the external milieu with subsequent uptake by the fungal cell. When the assay was repeated with bacterial and fungal cells separated by a cell-impermeable membrane, the number of recovered fungal cells was independent of the T6SS functionality of the underlying bacterial strain and comparable to that when placed directly on the media (Fig. 1a). Thus bacterial-fungal cell contact is essential for anti-fungal T6SS activity. Next, the range of fungal target cells was expanded to include pathogenic fungi, namely *Candida* species, clinically-important fungal pathogens commonly residing with bacteria in polymicrobial infection sites2, 13. We tested *Candida albicans*, the most frequently-isolated fungal pathogen in humans, and the phylogenetically-distant *Candida glabrata*, which displays intrinsic resistance to common anti-fungal drugs14. Both organisms were susceptible to T6SS-mediated anti-fungal activity, indicating a broad anti-fungal action of the *S. marcescens* T6SS (Fig. 1b).

Identification of two anti-fungal T6SS effector proteins

Having established fungi as a second target kingdom of the *S. marcescens* T6SS, we sought to identify the effector proteins responsible. The potential anti-fungal activity of six previously-identified T6SS-secreted proteins (Ssp1-612) was tested by utilising specific effector deletion mutants as attacker strains. Deletion of *SMDB11_1112* (*ssp3*) resulted in a 4-fold increase in recovery of viable *C. albicans* target cells compared with the wild type, although it had little effect on *S. cerevisiae* or *C. glabrata* (Fig. 1c). SMDB11_1112 was therefore renamed Tfe1 (T6SS anti-fungal effector 1). Subsequent deletion of five more effectors (mutant Δ*ssp1-6*) had no additional effect on the survival of fungal cells (Supplementary Fig. 1), suggesting the existence of further, unidentified T6SS-dependent effector(s).

To identify additional potential effectors, we employed a cellular proteomics approach, a complementary strategy to our previous secretome analysis, with the rationale that T6SS-secreted proteins would be retained inside the cell of a T6SS-inactive mutant. Using label-free quantitative mass spectrometry, we quantified 3034 proteins, representing 64% of the *S. marcescens* Db10 genome. Twelve proteins were identified as having significantly increased intracellular abundance in the Δ*tssE* mutant compared with the wild type (Fig. 2a, Supplementary Data 1, Supplementary Fig. 2). Nine were known secreted components or effectors of the T6SS machinery12, 15, including Tfe1, validating the approach. The remaining three proteins, of unknown functions, represented candidates for previously-undescribed T6SS effectors. Since, as a predicted lipoprotein, SMDB11_1031 is unlikely to be available for T6SS-dependent secretion, we focused on the two remaining candidates, SMDB11_1083 and SMDB11_3457, the latter encoded downstream of two Hcp homologues. Neither candidate is encoded adjacent to potential cognate immunity proteins (Fig. 2b). This non-compliance with one of the main criteria for anti-bacterial effectors8 further marked them as potential anti-fungal agents.

To determine whether SMDB11_1083 or SMDB11_3457 are T6SS-delivered anti-fungal toxins, the respective deletion mutants were used as attacking strains in bacterial-fungal co-cultures. Whereas loss of SMDB11_3457 did not have any effect on anti-fungal activity of *S. marcescens*, removal of SMDB11_1083 resulted in almost complete loss of activity

against *S. cerevisiae* or *C. glabrata* and reduced activity against *C. albicans* (Fig. 1c). SMDB11_1083 therefore represents a second T6SS-delivered anti-fungal effector, named Tfe2. When *C. albicans* was co-cultured with a mutant lacking Tfe1 and Tfe2, the partial anti-fungal activity seen with either single mutant was eliminated. Expression of Tfe1 and Tfe2 *in trans* was able to restore fungal inhibition in the respective deletion mutants (Fig. 1d). Overexpression of Tfe1 decreased anti-fungal activity against *S. cerevisiae* and *C. glabrata*, perhaps indicating that competition between Tfe1 and Tfe2 for the T6SS machinery resulted in reduced delivery of the more potent Tfe2. Finally, confirming that Tfe1 and Tfe2 are not required for T6SS function, mutants lacking Tfe1 and Tfe2 had no impairment in their ability to secrete the expelled component Hcp or the effector Ssp2 (Fig. 1e), or in anti-bacterial activity against *Pseudomonas fluorescens* (Supplementary Fig. 3).

Tfe1 can induce mild growth inhibition if overexpressed in bacterial cells, which is alleviated by co-expression with the immunity protein Sip312. However, in contrast to mutants lacking immunity proteins for true anti-bacterial effectors12, 15, 16, the Δ*sip3* mutant is fully fit and is not sensitive to the T6SS of the wild type or a Tfe1-overexpressing strain (Supplementary Fig. 3). These data suggest that the intended target of Tfe1 is not bacterial cells, but that Sip3 acts as a failsafe against non-specific toxicity should excess Tfe1 occur. For Tfe2, no anti-bacterial toxicity could be detected upon overexpression nor candidate immunity gene identified. Additionally, the *S. marcescens* T6SS, and by implication its effectors, does not appear to act against higher eukaryotic organisms, since T6SS-inactive mutants show no loss of virulence in several models (ref10, Supplementary Fig. 4). Taken together, we conclude that Tfe1 and Tfe2 are the major anti-fungal toxins deployed by the T6SS of *S. marcescens* and are likely to be used only against fungal cells.

Tfe1 and Tfe2 exhibit distinct anti-fungal activity

Bioinformatic analysis failed to reveal conserved domains or predicted functions for Tfe1 or Tfe2. Therefore their impact on fungal cell integrity was investigated following growth in co-culture with *S. marcescens*. With *C. albicans* as the target, cell distortion and lysis was detected, dependent on the T6SS and Tfe1 in the attacking bacteria (Fig. 3a). In agreement with these data, many necrotic *C. albicans* cells were observed by cryo-TEM following co-culture with wild type *S. marcescens*, whereas few such cells were seen with a T6SS-inactive mutant (Supplementary Fig. 5). With *S. cerevisiae* or *C. glabrata*, granular structures were observed in a T6SS- and Tfe2-dependent manner (Fig. 3a), consistent with the primary role of Tfe2 against both organisms in co-culture viability assays (Fig. 1). Propidium iodide (PI) stains cells which have lost the membrane permeability barrier, a common indirect proxy for loss of viability. We observed that ~50% of *C. albicans* and *C. glabrata* cells recovered from co-cultures with *S. marcescens* showed PI-staining, dependent on the T6SS and either Tfe1 (*C. albicans*) or Tfe2 (*C. glabrata*) (Fig. 3b). These observations are consistent with co-culture viable count assays (Fig. 1), where recovery of viable fungal cells co-cultured with wild type *S. marcescens* was lower than the initial inoculum, implying fungicidal action. In contrast, PI-staining was not observed in *S. cerevisiae*. To confirm directly that Tfe1 and Tfe2 possess intrinsic anti-fungal activity, and investigate further their impact on the different fungal species, each effector was expressed in *S. cerevisiae* and *C. albicans* using galactose- and doxycycline-inducible17 expression systems, respectively.

Expression of Tfe1, but not the anti-bacterial effectors Ssp1 and Ssp2, strongly inhibited growth of *S. cerevisiae* and induced abnormally large vacuoles and cell lysis (Fig. 3d,e; Supplementary Fig. 6), confirming the fungicidal potential of Tfe1. Similarly, expression of Tfe1 in *C. albicans* caused growth inhibition and cell death (Supplementary Fig. 7) and reproduced the Tfe1-dependent morphological changes observed in co-culture (Fig.3c). Expression of Tfe2 in *S. cerevisiae*, whilst not causing obvious changes in morphology, was able to abolish growth, even at very low levels (Fig. 3c,d).

Induction of Tfe2 during logarithmic growth of *S. cerevisiae* in liquid cultures resulted in a decline in the number of viable cells over time, whilst cell density approached steady-state. Upon removal of induction, yeast cells recovered from Tfe2-induced growth inhibition within 3 h to resume normal growth (Fig. 4a). These results indicate that Tfe2-mediated intoxication of *S. cerevisiae* primarily results in growth inhibition, with reduced long-term survival as a downstream consequence. To investigate whether the fungistatic effect of Tfe2 on *S. cerevisiae* was caused by inhibition of metabolic activity, the fluorescent dye FUN1 was utilised. Metabolically-active cells transport the dye into the vacuole where it forms distinct tubular structures which exhibit red fluorescence. In metabolically-inactive cells, the dye remains in the cytoplasm and fluoresces green18. Bright red structures, apparently vacuole-associated and similar to those observed in the control strain, were detected during early stages of Tfe1 expression when the cells gained dramatically in size (Fig. 4b), eventually being replaced by green fluorescence before onset of lysis. Tfe2-expressing cells also displayed bright red fluorescent structures, however, these appeared more globular, dispersed and mainly outside the vacuole. Together with the persistence of green fluorescence, this indicates that Tfe2 causes reduced cellular metabolic activity and potential interference with vacuolar transport19.

To determine whether either effector causes loss of plasma membrane potential, *S. cerevisiae* cells expressing Tfe1 or Tfe2 were stained with the voltage-dependent dye $DiBAC_4(3)$ which enters cells in a depolarisation-dependent manner. Tfe1 intoxication resulted in membrane depolarisation, similar to treatment with mellitin and amphotericin B, whereas Tfe2 caused no loss of membrane potential (Fig. 4c). Co-staining with PI revealed that only a fraction of the Tfe1-intoxicated cells showing depolarisation also exhibited a loss of membrane integrity, in contrast with the action of the pore-forming peptide mellitin where all depolarised cells were also permeabilised (Fig. 4d, Supplementary Fig. 8). Intoxication of *C. albicans* by T6SS-delivered Tfe1 caused a similar pattern of membrane depolarisation and selective permeability (Supplementary Fig. 9). Thus our data suggest that Tfe1 primarily causes a loss of membrane potential, which is not due to pore formation but can ultimately lead to a loss of membrane integrity, and imply that Tfe1 and Tfe2 act on different cellular targets in fungal cells.

The T6SS can act on filamentous fungal cells

Whilst *P. aeruginosa* has been reported to preferentially kill the hyphal form of *C. albicans*20, we had so far demonstrated T6SS activity against the budding yeast form. Co-culture of *S. marcescens* with the constitutively filamentous *tup1*Δ mutant21 revealed PI-staining of individual cell segments within filaments, with this localised action being

dependent on the T6SS and Tfe1 (Fig. 4e,f). A T6SS- and Tfe1-dependent drop in viable cell counts was also observed (Supplementary Fig. 10). Thus the anti-fungal *S. marcescens* T6SS can intoxicate budding and filamentous forms of *C. albicans.*

'In competition' proteomics reveals that T6SS-delivered Tfe2 disrupts nutrient transport and metabolism and induces autophagy

To identify specific cellular pathways affected by the anti-fungal effectors in a physiologically-relevant context, namely when delivered by the T6SS, we performed 'in competition' proteomics using *C. albicans* as target. Fungal cells were co-cultured with wild type *S. marcescens* Db10, the T6SS-inactive mutant Δ*tssE,* or effector mutants, Δ*tfe1*, Δ*tfe2* and Δ*tfe1*Δ*tfe2*, before performing quantitative mass spectrometric analysis of the total fungal proteome in each condition using isotope-labelled tandem mass tags (six-plex TMT). 4446 *C. albicans* proteins (~72% of the genome) and 2486 *S. marcescens* proteins were quantified (Supplementary Data 2, Supplementary Fig. 11-15). Of the *C. albicans* proteins, 1667 showed significant modulation across the five-way comparison (ANOVA-positive, $p<0.05$). Hierarchical clustering of these modulated proteins confirmed that Tfe1 and Tfe2 cause disruption of different fungal pathways. The analysis also demonstrated that the major response of *C. albicans* is to T6SS-dependent translocation of Tfe2, since the response to the Δ*tfe2* mutant was similar to that of Δ*tssE* or Δ*tfe1*Δ*tfe2* (Fig. 5a). To identify individual proteins within this set as being robustly altered in specific response to Tfe2, we further imposed requirements for a significant change in abundance (>1.3-fold) to be observed in the presence of the wild type compared with the Δ*tfe2* mutant, and for a consistent change to be observed in Δ*tfe1*Δ*tfe2* and Δ*tssE* mutants. According to these criteria, 14 fungal proteins were upregulated in response to Tfe2 delivery and 16 downregulated (Supplementary Table 1). In contrast, no Tfe1-specific proteins were identified using these strict criteria. This may, at least in part, reflect Tfe1 acting on a non-protein target, consistent with its ability to induce plasma membrane depolarisation. Evaluation of the 30 Tfe2-responsive proteins by Gene Ontology enrichment analysis identified significant overrepresentation of proteins belonging to the cellular amino acid biosynthetic process (GOID 8652), specifically arginine biosynthesis (GOID 6526) and sulfur amino acid biosynthesis (GOID 0097), as well as anion transport (GOID 6820) (Fig. 5b; see also Supplementary Table 2). Therefore subsequent analysis was focused on these areas of nutrient uptake and amino acid metabolism.

Fungal cells must acquire sulfur from their environment for the *de novo* biosynthesis of cysteine, methionine and other organic sulfur metabolites, such as glutathione22. The sole sulfate transporter in *C. albicans*, Sul2, and members of the sulfate assimilation pathway were strongly decreased in the presence of Tfe2-translocating bacteria. Heat map analysis of relevant proteins revealed downregulation of the entire pathway for reduction of inorganic sulfate to homocysteine in response to Tfe2 (Fig. 5c). Similar to Sul2, two general amino acid permeases, Gap1 and Gap2, and two basic amino acid permeases, Can1 and Can2, all of which transport arginine into the fungal cell23–25, were subject to Tfe2-dependent downregulation (Fig. 5d). Furthermore, examination of arginine metabolic proteins26 in the proteomics dataset indicated Tfe2-dependent accumulation of proteins involved in arginine synthesis, whereas proteins mediating arginine catabolism were unchanged or decreased

(Fig. 5d). Consistent with this profile, intracellular arginine levels in *S. cerevisiae* expressing Tfe2 were increased 4-fold compared with control cells (Fig. 6a). Lysine levels were also increased, and a further 14 amino acids displayed a range of down- or upregulation, indicating extensive nutrient imbalance upon Tfe2-mediated intoxication.

Next, we determined if Tfe2-induced reduction of fungal nutrient transporters, which also included the peptide transporter Ptr22 (Supplementary Table 1), is due to transcriptional downregulation. Plasma membrane transporter expression is induced by substrate, which is sensed by the transporter itself, as for Sul2, or by non-transporting membrane proteins, including the amino acid sensor Csy1 (Ssy1 in *S. cerevisiae*), a component of the SPS sensing complex27, 28. Transcript levels of the sensor gene *SSY1*, SPS-activated transcriptional regulators *STP1* and *STP2*, and SPS-controlled permease genes29–31 were increased upon expression of Tfe2 in *S. cerevisiae* (Fig. 6b). This implies that Tfe2 does not inhibit SPS sensing or signalling. Rather, transcriptional induction of the SPS-regulon is consistent with Tfe2-induced intracellular nutrient depletion or imbalance. Similarly, sulfate transporter transcript levels were upregulated by Tfe2, despite downregulation at the protein level. We confirmed that T6SS-mediated delivery of Tfe2 decreases levels of Can1 in *S. cerevisiae*, with redistribution from the plasma membrane suggesting vacuolar degradation (Supplementary Fig. 16). These data indicate that Tfe2 intoxication causes depletion of nutrient transporters at a post-transcriptional level. In turn, the resulting decrease in intracellular nutrients may lead to downregulation of nutrient-utilisation pathways, as observed for proteins of the sulfate assimilation pathway (Fig. 5c), or in upregulation of compensatory metabolic pathways, as observed for arginine synthesis (Fig. 5d).

Further evidence for Tfe2-dependent interference with the intracellular amino acid pool was the marked increase in the bZip transcriptional activator protein Gcn4 (Supplementary Table 1), which mediates the general amino acid control (GAAC) response to amino acid starvation32, 33. The proteomics data also revealed a Tfe2-dependent increase in the levels of Atg1, a Ser/Thr kinase subject to regulation by the nutrient-sensing TOR signalling pathway. Activation of Atg1 by phosphorylation in response to nitrogen and amino acid starvation leads to induction of autophagy34. To investigate if Tfe2-mediated amino acid limitation leads to autophagy, we analysed proteolytic processing of the autophagy reporter protein GFP-Atg835, 36 in *S. cerevisiae* co-cultured with *S. marcescens*. With yeast alone, only full length GFP-Atg8 was observed. Upon co-culture with wild type *S. marcescens*, a band corresponding to free GFP was detected, indicating processing of GFP-Atg8 by vacuolar peptidases and thus induction of autophagy. Processing was not detected upon co-culture with bacteria lacking Tfe2 or a functional T6SS, nor in cells lacking the key autophagy regulator, Atg13 (Fig. 6c, Supplementary Fig. 17). Hence induction of autophagy is dependent on T6SS-mediated delivery of Tfe2. Although Tfe2 may induce autophagy independent of amino acid imbalance, our results are consistent with the idea that Tfe2-mediated intoxication of fungal cells leads to disruption of the intracellular amino acid pool, causing a starvation signal which induces autophagy as a protective response.

Overall, we have revealed that Tfe2 intoxication leads to extensive nutrient imbalance, interference with plasma membrane transporters and induction of autophagy. The precise aspect or combination of these factors which ultimately leads to the death of the fungal cell

remains to be deciphered. In contrast, Tfe1 acts via a plasma membrane depolarising mechanism which does not involve formation of large, unselective pores.

Discussion

Cellular proteomics combined with genetic analysis led us to discover the first T6SS-dependent anti-fungal effectors, Tfe1 and Tfe2, whose T6SS-dependent secretion was confirmed in our concurrent secretome study15. The two effectors elicit distinct responses in fungal cells and can exert a fungicidal effect. The severity of the fungal response to each toxin differs between species, likely reflecting divergence of metabolic pathways. 'In competition' proteomics revealed that T6SS-delivered Tfe2 disrupts fungal nutrient uptake and metabolism. In particular, Tfe2 intoxication strongly affected inter-related pathways involved in sulfate assimilation, plasma membrane nutrient transport and amino acid metabolism and also caused induction of autophagy. Autophagy is a process by which, under nutrient-limiting stress conditions, fungal cells target cellular macromolecules for vacuolar degradation and recycling34, 37. Induction of this pathway in response to Tfe2 indicates severe disturbance of the intracellular metabolic equilibrium and may represent a protective response attempting to rescue the viability of the fungal cell. A striking change in response to Tfe2 was increased intracellular levels of arginine and lysine. Upregulation of arginine and lysine synthesis has been linked to sudden nutrient limitation upon engulfment by neutrophils38, 39, and regulation of arginine synthesis in response to phagocytosis may also represent a protective mechanism against the phagocyte oxidative burst in *C. albicans* 40, 41. Thus Tfe2 may be causing a similar response to that induced upon phagocytosis. Tfe1, in contrast, does not provoke a strong proteomic response and instead causes plasma membrane depolarisation, reminiscent of T6SS-delivered antibacterial effectors which target the bacterial membrane8.

This study demonstrates that the bacterial T6SS can act as a potent anti-fungal weapon, causing growth arrest and death of fungal cells. In agreement with the prevailing model, T6SS-dependent anti-fungal activity required attacker-target cell-cell contact, suggesting that effector translocation occurs directly into the fungal cell. Supporting the feasibility of this idea, cryo-TEM showed an intimate interaction between cells of *C. albicans* and *S. marcescens* (Supplementary Fig. 5). Moreover, the expelled arrow-like structure of the T6SS should have both the length (approximately 0.7 μm, at least three times the thickness of the average fungal cell wall)42–44 and the force4 to puncture the rigid fungal cell wall. The *S. marcescens* T6SS delivers multiple anti-bacterial effectors and is a potent weapon against competitor bacteria10. However this study reveals a second, prominent role for this T6SS in controlling growth of co-habiting fungal micro-organisms. Whilst *Serratia-Candida* interactions may on occasion be relevant clinically, given that both can colonise common sites such as bloodstream, respiratory, and GI tracts2, 45, 46, *Serratia* is ubiquitous in the environment and likely uses its anti-fungal T6SS in diverse contexts. More importantly, our work implies that other bacterial pathogens may deploy a T6SS against fungal cells during polymicrobial infection. This is supported by the observation that Tfe2 homologues are present in other pathogenic T6SS-containing bacteria, including *Pseudomonas* and *Vibrio* species. Thus, we propose that anti-fungal T6SS activity is widespread and may be an intrinsic property of many, if not all, 'anti-bacterial' T6SSs. Indeed, one report has suggested

anti-yeast activity associated with a T6SS in *P. syringae*, although no effectors were identified47. The fact that T6SS anti-fungal effectors have not been discovered previously may be partially attributable to many identification strategies relying on the presence of associated immunity proteins, therefore excluding proteins such as Tfe2.

With the identification of a previously-undescribed class of effectors, anti-fungal toxins, we have expanded the repertoire of the T6SS arsenal to include another target kingdom and highlighted another role for this versatile machinery in shaping polymicrobial communities. Deployment of T6SSs enabling simultaneous attack upon prokaryotic and fungal rivals should represent a key determinant of bacterial competitive fitness in a multitude of environments, from rhizosphere to polymicrobial human infections.

Methods

Bacterial strains, plasmids and culture conditions

Bacterial strains and plasmids used in this study are given in Supplementary Table 3. Mutant strains of *S. marcescens* Db10 carrying in-frame deletions were generated by allelic exchange using the pKNG101 suicide vector, and effector genes were cloned into pSUPROM for constitutive expression *in trans*10. To avoid non-specific anti-bacterial toxicity upon complementation of the Δ*tfe1* strain by plasmid-encoded Tfe1, the cognate immunity gene *sip3* was included in the construct. All primer sequences for mutant and plasmid generation are given in Supplementary Table 4. Strains of *S. marcescens* were grown at 30°C in LB media (10 g/l tryptone, 5 g/l yeast extract, 10 g/l NaCl), solidified with 12 g/l agar or supplemented with antibiotics (kanamycin, 100 μg/ml; streptomycin, 100 μg/ml) where required.

Fungal strains, plasmids and culture conditions

Fungal strains and plasmids are given in Supplementary Table 3. To generate mutant strains of *S. cerevisiae* K699 carrying chromosomal insertions of GFP or bacterial effector genes under the control of the P_{GAL1} promoter, linearized plasmids pSC1384 (control), pSC1379 (GFP), pSC1382 (Tfe1) and pSC1380 (Tfe2), all based on plasmid pGED1, were integrated by allelic exchange into the HIS3 locus. Plasmid-based gene expression utilised the galactose-inducible vector pRB1438. For *in trans* expression of bacterial effectors in *C. albicans*, chromosomal integration mutants based on the doxycycline-inducible expression vector pNIM117 were generated. To ensure correct leucine incorporation into the expressed protein in *C. albicans*, synthetic genes carrying CTG to TTG substitutions (Invitrogen) were subcloned into pNIM1. Correct sequence and locus integration was confirmed by sequencing of the respective PCR product, together with Southern blot analysis for *C. albicans*. All primer sequences for mutant and plasmid generation and Southern blot probe generation are given in Supplementary Table 4. Fungal strains were cultured at 30°C in YPDA (10 g/l yeast extract, 20g/l peptone, 40 mg/l adenine hemisulfate) or synthetic complete (SC; 6.9 g/l yeast nitrogen base complete with ammonium sulfate and amino acids) media containing 2% glucose48. If utilizing auxotrophies, SC media lacking the respective amino acid or nucleotide was used. For induction of the P_{GAL1} promoter, *S. cerevisiae* cultures were pre-incubated in media containing 2% raffinose, washed, and

incubated with media containing both 2% galactose and 2% raffinose unless otherwise stated. Induction of the Tet-inducible promoter in *C. albicans* was by addition of 50 μg/ml doxycycline.

Co-culture assay for T6SS-mediated anti-fungal activity

Anti-fungal activity assays were based on the anti-bacterial co-culture assay described previously10. Both the attacker strain derived from *S. marcescens* Db10 and the respective fungal target strain were normalized to an OD_{600} of 1, mixed at a volume ratio of 1:1 (attacker:target cell ratio ~100:1), and 12.5 μl of the mixture were spotted on solid SC + 2% glucose media and incubated for 7.5 h at 30°C. Surviving target fungal cells were enumerated by serial dilution and viable counts on streptomycin-supplemented YPDA media. Co-culture assays for anti-bacterial activity were performed as described10, 16. For assessment of cell contact dependence, bacterial and fungal cells were separated by a membrane (pore size 0.22 μm), with the bacterial layer between the solid medium and the membrane and the fungal cells spotted on top of the membrane. *S. cerevisiae* grew equally well on the membrane placed on top of the bacterial cell layer compared with direct growth on the medium, confirming efficient diffusion of nutrients through the membrane. The co-culture experiments presented contain data from four independent biological replicates, performed on at least two days, with T6SS-dependent anti-fungal activity and the phenotypes of the Δ*tfe1* and Δ*tfe2* mutants having been confirmed on multiple independent occasions.

Plate toxicity assay

Fungal cells were pre-grown in non-inducing liquid minimal media (SC + 2% glucose, *C. albicans*; DOA-LEU + 2% raffinose, *S. cerevisiae*) at 30°C, adjusted to an OD_{600} of 1, serially diluted and 5 μl spotted onto minimal media agar. Heterologous protein expression was induced by addition of doxycyline (50 μg/ml, *C. albicans*) or galactose (0.008 – 0.2%, *S. cerevisiae*). Agar plates were incubated at 30°C and pictures taken after 48 h (*C. albicans*) or 96 h (*S. cerevisiae*).

Cell morphology and viability analysis by microscopy

Single cell morphology of fungal cells grown in co-culture (7.5 h) or in liquid induction media (SC + 2% glucose + 50 μg/ml doxycycline, *C. albicans*; DOA-URA + 2% raffinose + 2% galactose, *S. cerevisiae*; 8h) was visualized by differential interference contrast (DIC) using a Axio-Imager M1 microscope equipped with a 100x objective, AxioCam MRm camera and ZEN software (Zeiss). The images presented show multiple individual cells from part of one field of view, for clarity, and are representative of between 9 and 42 fields of view, acquired on three separate occasions. To determine the percentage of propidium iodide (PI)-stained fungal cells, cells from three independent fungal-bacterial co-cultures grown at 30°C for 7.5 h on solid SC + 2% glucose media were recovered in 1x PBS and stained with PI at a final concentration of 10 μg/ml. Following a 15 min incubation at 30°C, 1.5 μl of the stained cell suspension were placed on a microscope slide layered with a 1% agarose pad and cells were detected by both DIC and fluorescence microscopy using a HBO 100 mercury lamp and appropriate filter sets (Ex 546/12 nm, Em 607/65 nm) and 40x objective. A minimum of 160 cells per experimental condition and replicate were scored, with the aid

of the counting tool in OMERO.mtools49. Cells subjected to a 40 min heat-shock at 65°C served as positive control for PI staining. Visualisation of *C. albicans* hyphae was performed using a Zeiss Axioskop 2 MOT microscope, 63x objective, HBO100 mercury lamp and Zeiss Axiocam Color camera, following incubation with 1 μM PI for 10 min. Microscopy images were managed and processed according to accepted standards using OMERO (http://openmicroscopy.org)49 and Fiji50.

Microscopy analysis of metabolic activity and membrane potential

For staining of effector-expressing *S. cerevisiae* cells using FUN1, cells were grown in synthetic drop-out media (DOA-LEU) supplemented with 2% raffinose, washed once, normalized to an OD_{600} of 0.5 and expression induced by addition of 2% galactose for 9 h. Cells were washed, suspended in 10 mM HEPES, pH 7.2, 2% raffinose, 2% galactose, stained with FUN1 (Thermo Fisher, dilution 1:1;000) for 30 min at 30°C, and analysed by DIC and fluorescence microscopy using appropriate filter sets (green, Ex 470/40 nm, Em 525/50 nm, 40 ms exposure; and red, Ex 546/12 nm, Em 607/65 nm, 150 ms exposure) on the Axio-Imager described above. Multiple fields of view were imaged and the experiment has been reproduced on an independent occasion.

To visualise and distinguish between changes in plasma membrane potential and membrane diffusion barrier function, *S. cerevisiae* cells grown in liquid induction media (DOA-URA + 2% raffinose + 2% galactose; 6 h) were placed on a microscope slide layered with a 1% agarose pad containing the voltage-dependent dye Bis-(1,3-dibutylbarbituric acid) trimethine oxonol [$DiBAC_4(3)$] (AnaSpec) at a final concentration of 10 μM, either alone, or combined with the membrane permeability-reporter PI (Sigma) added at a final concentration of 1 μM. To suppress binding of $DiBAC_4(3)$ on the glass surface, the coverslips were coated with L-dopamine51. Amphotericin B (Sigma), used as positive control to induce membrane depolarization without pore formation, was added to control cells at the start of the 6 h induction period at a final concentration of 3 μg/ml. The pore-forming peptide mellitin (AnaSpec) was added to the cells 10 min prior to the end of the 6 h induction period at a final concentration of 10 μM. Fluorescence and phase contrast microscopy was carried out with Nikon Eclipse Ti equipped with Nikon Plan Apo 100x/1.40 Oil Ph3 objective, Sutter Instrument Company Lambda LS xenon arc light source, and Photometrics Prime sCMOS camera using appropriate filter sets (green Ex 470/40 nm, Em 525/50 nm, 500 ms exposure; and red Ex 560/40 nm, 630/40 nm, 100 ms exposure). The images were captured using Metamorph 7.7 (Molecular Devices). Multiple fields of view were imaged and the experiment has been reproduced on an independent occasion. The quantification of cell fluorescence levels was performed by automated detection of cells using phase contrast images, followed by measurement of whole cell $DiBAC_4(3)$ and PI average fluorescence intensities from corresponding, background-subtracted fluorescent micrographs. The cell detection and fluorescence intensity measurements were carried out using Fiji50.

Microscopy analysis of Can1-GFP localisation in in *S. cerevisiae*

To determine cellular localization of fungal Can1-GFP upon co-culture with *Serratia*, yeast-bacterial co-cultures were resuspended into SC media, incubated for 10 min at 30°C with the fluorescent dye CellTracker™ Blue CMAC (Thermo Fisher) at a final concentration of 100

μM, washed once and mounted on 1% agarose pads. The fluorescent and phase contrast images were captured with Nikon Eclipse Ti equipped with Nikon Plan Apo 100x/1.40 Oil Ph3 objective, Sutter Instrument Company Lambda LS xenon arc light source, and Photometrics Prime sCMOS camera using appropriate filter sets (blue Ex 350/50 nm, Em 460/50 nm, 1 s exposure; green Ex 470/40 nm, Em 525/50 nm, 1 s exposure). The images were captured using Metamorph 7.7 (Molecular Devices). Multiple fields of view were imaged and the experiment has been reproduced on an independent occasion. The quantification of the Can1-GFP fluorescence emitted from the plasma membrane under the different experimental conditions was carried out by randomly selecting 30 individual cells based on phase contrast images, followed by measurement of plasma membrane and cell interior fluorescence signals from the corresponding, background-subtracted fluorescent micrographs. The plasma membrane signal was measured as the average signal intensity of the cell area corresponding to a manually drawn 6-pixel wide line tracing the cell edge. The interior fluorescent signal was measured as the average signal intensity of the whole cell area, as determined by manually tracing and excluding the cell periphery. The determination of the measurement areas, and the quantification of the corresponding average fluorescence levels were carried out with Fiji50.

Cryo-Transmission Electron Microscopy

S. marcescens and *C. albicans* were co-cultured as above. High Pressure Freezing was carried out using a Leica EM PACT 2 (Leica Microsystems, Milton Keynes, UK) and samples were freeze substituted in a Leica AFS 2. Freeze substitution was carried out using the following program: -95°C to -90°C for 30 h with 2% OsO4 in acetone, -90°C for 10 h with 2% OsO4 in acetone, -90°C to -30°C for 8 h with 2% OsO4 in acetone, -30°C to -10°C for 1 h with acetone, -10°C to 4°C for 1 h in acetone, 4°C to 20°C for 1 h in acetone. Samples were then placed in 10% Spurr's (TAAB, UK): acetone for 72 h, followed by 30% Spurr's overnight, 50% Spurr's for 8 h, 70% Spurr's overnight, 90% Spurr's for 8 h and embedded in Spurr's resin at 60°C for at least 24 h. Ultrathin sections were cut to 90 μm using a diamond knife (Diatome Ltd, Switzerland) onto copper grids (TAAB, UK) using a Leica UC6 and were contrast stained with uranyl acetate and lead citrate in a Leica AC20. Samples were imaged on a JEM 1400 plus (JEOL UK) Transmission Electron Microscope and captured using an AMT UltraVUE camera (AMT, USA).

Immunoblot analysis

Anti-Hcp and anti-Ssp2 immunoblots were performed on cultures grown for 5 h as previously described10, 16. Polyclonal anti-Hcp10 and anti-Ssp216 primary antibodies were used at 1:6,000 and 1:2,000 respectively, with peroxidase-conjugated anti-rabbit secondary antibody (BioRad) at 1:10,000. Cellular samples for immunodetection of GFP-Atg8 and corresponding Pgk1 control were prepared from yeast-bacterial co-cultures based on52. Yeast cells were harvested from co-cultures grown at 30°C for 7.5 h on solid DOA-URA media into ice-cold phosphate buffered saline (PBS; 8 g/l NaCl, 0.2 g/l KCl, 1.42 g/l Na_2HPO_4, 0.24 g/l KH_2PO_4, pH 7.4), washed twice by filtering through 3 μm pore-sized PVDF membranes (Millipore) and recovered by centrifugation. For subsequent protein extraction, cell pellets were resuspended and incubated for 10 min in 0.2 M NaOH, 1% β-mercaptoethanol. Proteins were precipitated by addition of trichloroacetic acid (TCA; 20%

final concentration), washed once in ice-cold acetone, resuspended in 2x SDS sample buffer (100 mM Tris-HCl, pH 6.8, 3.2% SDS, 3.2 mM EDTA, 16% glycerol, 0.2 mg/ml bromophenol blue and 2.5% β-mercaptoethanol) and boiled for 10 min. Cellular samples for immunodetection of Can1-GFP and corresponding Pgk1 control were prepared from yeast-bacterial co-cultures based on53. Yeast cells were harvested from co-cultures grown at 30°C for 7.5 h on solid SC + 2% glucose media into ice-cold PBS, washed twice by filtering through 3 μm pore-sized PVDF membranes and recovered by centrifugation. For subsequent protein extraction, cell pellets were resuspended in 10% ice-cold TCA, washed twice in acetone and resuspended in MURB-based buffer (25 mM MOPS, 50 mM phosphate buffer, pH 7.0, 3M urea, 1 % SDS, bromophenol blue, 1 mM NaN_3, 0.5% β- mercaptoethanol). This was followed by disruption with approximately one-half volume of acid-washed glass beads using a Mini-BeadBeater-16 (BioSpec Products) (5x 30 seconds with 30 seconds intervals). Samples were separated by SDS-PAGE and subjected to immunoblotting. For GFP-ATG8 and Can1-GFP experiments, due to the growth impediment of *S. cerevisiae* in the presence of *S. marcescens* Db10 and residual bacterial contamination of yeast samples, protein extracts were normalized according to the abundance of the protein Pgk1. Monoclonal anti-GFP (cat # 11814460001, Roche) and polyclonal anti-Pgk1 (cat # 13472727, Invitrogen) primary antibodies were used at 1:5,000 and 1:1,000 respectively, with peroxidase-conjugated anti-mouse and anti-rabbit secondary antibodies (BioRad) at 1:10,000. Visualisation utilised conventional ECL and X-ray film, except in the case of Can1-GFP where the same membrane was then reprobed with anti-Pgk1 and visualised using a Typhoon imaging system (GE Healthcare).

Quantitative real-time PCR

RNA was extracted from three independent cultures of control and Tfe2-expressing *S. cerevisiae* cells, induced for 6 h at 30°C in galactose induction media, using the SV Total RNA Isolation System (Promega), followed by treatment with the Turbo DNA-free kit (Ambion) to remove residual gDNA. RNA was reverse transcribed using the iScript cDNA Synthesis Kit (Bio-Rad) and relative levels of cDNA determined using an Mx3005P QPCR machine (Stratagene, Agilent Technologies) with actin (*ACT1*) as the normalizing gene. Primer sequences are given in Supplementary Table 4. The experiment presented has been reproduced on an independent occasion.

Whole-cell amino acid analysis

Three independent cultures of control and Tfe2-expressing *S. cerevisiae* cells were incubated for 6 h at 30°C in galactose induction media, washed twice with ice-cold water, normalized to 5 OD_{600} per 1 ml of water and boiled for 15 min. After centrifugation, the supernatant was clarified using a 0.2 μm syringe filter (Sartorius). The resulting extract was acidified by addition of TFA in MeOH (10%, v/v), dried and resuspended in buffer (40% 1M NaOAc, 40% MeOH, 20% triethylamine, TEA), before being dried again. The amino acids were then derivatized using Phenylisothiocyanate (PITC) by resuspension of the dried material in 10% PITC, 70% MeOH, 10% H_2O, 10% TEA, followed by 2-fold dilution in MeOH. After 15 min incubation at room temperature, suspensions were dried, washed once with MeOH and suspended in elution buffer, composed of 95% (150 mM NaOAc, 0.5 ml/l TEA, pH 6.4) and 5% acetonitrile. PTC amino acid derivatives were analysed by HPLC using a Nova-Pak®

C18 column (Waters), the Clarity Lite software and two amino acid standard sets (AA-S-18 and A6282, Sigma). The experiment presented has been reproduced on two independent occasions.

Infection of RAW264.7 cells with *Serratia marcescens*

Murine macrophage-like cells RAW264.7 were cultured in Dulbecco's Modified Eagle's medium GlutaMax (Invitrogen) supplemented with 10% foetal bovine serum (Sigma) and grown at 37 °C, 5% CO_2. RAW264.7 cells were cultured in 24-well plates at a density of 200,000 cells per well for 24 h prior to the infection assay. RAW264.7 cells were infected with strains of *S. marcescens* at a multiplicity of infection of 10 for 2 h, 4 h, and 6 h. The morphology of RAW264.7 cells was monitored during the course of infection and culture supernatants were collected at each time point for the cytotoxicity assay. Within each independent experiment, an infection with each bacterial strain was performed in duplicate cell culture wells (technical replicate). To measure cytotoxicity, culture supernatants, isolated by centrifugation at 14,000 rpm for 2 min, were analysed for the presence of lactate dehydrogenase (LDH) using the Pierce LDH cytotoxicity assay kit (Thermo Fisher). Cytotoxicity (%) was determined by the quantification of LDH release in the culture supernatant relative to total cellular LDH release from complete cell lysis with 0.1% Triton X-100 (100%). Derivatives of *S. marcescens* Db10 and SJC11(Δ*tssE*) lacking production of secreted haemolysin were generated by introduction of the *shlB*::miniTn*5*-Cm insertion from strain 21C454 by generalised transduction using ΦIF355. RAW264.7 cells were obtained from ATCC. The stock has been authenticated previously by proteomics and has been tested regularly for mycoplasma contamination.

Sample preparation for mass spectrometry

For analysis of the cellular proteome of *S. marcescens*, six biological replicates of each strain (two spots of 25 µl of OD_{600} 0.5 per replicate) were grown on solid LB media for 7.5 h at 30°C. Cells were recovered, washed in ice-cold PBS, resuspended in 1% sodium 3-[(2-methyl-2-undecyl-1,3-dioxolan-4-yl)methoxy]-1-propanesulfonate (commercially available as RapiGest, Waters, Milford, MA), 50 mM Tris-HCl pH 8.0, 1 mM tris(2-carboxyethyl)phosphine (TCEP) and lysed by sonication.

For analysis of bacterially-intoxicated fungal cells, co-cultures of *C. albicans* and *S. marcescens* (57 co-culture spots, inoculated as above, per replicate) were incubated on solid SC + 2% glucose media for 4 h at 30°C, with six biological replicates per combination. Cells were harvested in 40 ml ice-cold PBS, washed 2x by filtration using PVDF membranes, pore size 3 µm (Millipore), suspended in PBS and recovered by centrifugation. Cells were sonicated in 1% Rapigest, 50 mM Tris-HCl pH 8.0, 1 mM TCEP in the presence of 0.1 mm zirconia/silica beads (BioSpec) for 6x 10 sec with 20 sec intervals. In each study, following sonication, samples were heated for 5 min at 95°C and soluble protein extracts recovered by centrifugation.

Protein concentrations were determined using the EZQ Kit (Thermo-Fisher Scientific) and cysteines were alkylated by addition of 5 mM iodoacetamide. After 20 min incubation in the dark at 25°C, the reaction was quenched by addition of 5 mM DTT and samples were

Europe PMC Funders Author Manuscripts

diluted 10x in 50 mM Tris-HCl pH 8.0. Digestion of proteins was by addition of trypsin (MS grade, Pierce, Thermo-Fisher) at a 1:150 (w/w) ratio with incubation overnight at 37°C, followed by a second addition of trypsin (1:150 w/w) with 3 h incubation. Rapigest was cleaved by addition of 2% trifluoroacetic acid (TFA) and incubation for 1 h at 37°C. Samples were desalted using C18 columns (Harvard Apparatus) and lyophilised.

Mass spectrometry analysis of *Serratia marcescens* cellular proteome

Lyophilised peptide samples (six biological replicates) were taken up in 2% acetonitrile (ACN), 0.1% TFA and analysed similar to previously published methods56–58: separated on an Ultimate 3000 RSLC system (Thermo-Fisher Scientific) with a C18 PepMap, serving as a trapping column (2 cm x 100 μm ID, PepMap C18, 5 μm particles, 100 Å pore size) followed by a 50 cm EASY-Spray column (50 cm x 75 μm ID, PepMap C18, 2 μm particles, 100 Å pore size; Thermo-Fisher Scientific) with a 6 h gradient consisting of 3-30% B (B= 80% ACN, 0.1% formic acid (FA); 10-260 min), to 40% B (330 min), 99% B (335-345 min), 3% (350-360 min) at 300 nl/min. Mass spectrometric identification and quantification was performed on an Orbitrap Velos mass spectrometer (Thermo-Fisher Scientific) operated in data dependent, positive ion mode. FullScan spectra were acquired in a range from 350 m/z to 1600 m/z, at a resolution of 60,000. MS/MS in the ion trap was triggered for ions above 2000 with a maximum injection time of 10 ms for the 20 most intense precursor ions in RapidScan and a lockmass of 445.120024. Collision-induced dissociation (CID) fragmentation was performed at a collision energy of 35% and 0.25 activation Q.

Label-free protein identification and quantification were performed using MaxQuant version 1.4.1.259 with the following parameters: stable modification carbamidomethyl (C); variable modifications oxidation (M), acetylation (protein N terminus), and trypsin as enzyme with 2 missed cleavages. Search was conducted using a combined FASTA database of *Serratia marcescens* Db11 and the Uniprot *Homo sapiens* database (downloaded May 1st 2013), including common contaminants. Mass accuracy was set to 4.5 ppm for precursor ions and 0.5 Da for ion trap MS/MS data. Identifications were filtered at a 1% false-discovery rate (FDR) at the protein and peptide level, accepting a minimum peptide length of 7 amino acids. Quantification of identified proteins referred to razor and unique peptides, and required a minimum ratio count of 2. Normalized ratios were extracted for each protein and were used for downstream analyses.

‘In competition’ proteomics of bacterially-intoxicated *C. albicans*

Isobaric labelling of peptides was performed using 6-plex tandem mass tag (TMT) reagents (Thermo-Fisher Scientific). TMT reagents (0.8 mg) were dissolved in 40 μl of acetonitrile and 20 μl was added to six biological replicates of lyophilised peptide samples, previously dissolved in 50 μl of 50 mM triethylammonium bicarbonate, pH 8.0. The individual samples of the strains were labelled as follows for all six replicates: WT, 126; Δ*tssE*, 127; Δ*tfe1*, 128; Δ*tfe2*, 129; Δ*tfe1*Δ*tfe2*, 130. After labelling, the reaction was quenched by addition of 4 μl of 5% hydroxylamine after 1 hour incubation at room temperature. Individual samples were tested for labelling efficiency (>95%) before the labelled peptides were combined, acidified with 0.1% TFA and concentrated using C18 SPE on Sep-Pak cartridges (Waters). Equal

loading of all five conditions was confirmed by the majority of peptide intensities not changing before normalisation.

TMT labelled peptides were subjected to hydrophilic Strong Anion Exchange (hSAX) fractionation.60 Labelled peptides were solubilized in 20 mM Tris-HCl, pH 10.0) and separated on a Dionex RFIC IonPac AS24 column (IonPac series, 2 × 250 mm, 2000 Å pore size; Thermo-Fisher Scientific). Using a DGP-3600BM pump system equipped with a SRD-3600 degasser (Thermo-Fisher Scientific) a 30 min gradient length from 8% to 80% of 1M NaCl in 20 mM Tris-HCl, pH 10 (flow rate of 0.25 ml/min), separated the peptide mixtures into a total of 34 fractions. The 34 fractions were merged into 9 samples, acidified with 1 %TFA (pH = 2), desalted via C18 Macro SpinColumns (Harvard Apparatus), dried under vacuum centrifugation and re-suspended in 2% ACN / 0.1% TFA for LC-MS/MS analysis.

Peptide samples were separated on an Ultimate 3000 RSLC system with a C18 PepMap, serving as a trapping column (2 cm x 100 μm ID, PepMap C18, 5 μm particles, 100 Å pore size) followed by a 50 cm EASY-Spray column with a linear gradient consisting of (2.4-28% ACN, 0.1% FA) over 150 min at 300 nl/min. Mass spectrometric identification and quantification was performed on an Orbitrap Fusion Tribrid mass spectrometer (Thermo-Fisher Scientific) operated in data dependent, positive ion mode. FullScan spectra were acquired in a range from 400 m/z to 1500 m/z, at a resolution of 120,000, with an automated gain control (AGC) of 300,000 ions and a maximum injection time of 50 ms. The 12 most intense precursor ions were isolated with a quadrupole mass filter width of 1.6 m/z and CID fragmentation was performed in one-step collision energy of 32% and 0.25 activation Q. Detection of MS/MS fragments was acquired in the linear ion trap in a rapid mode with an AGC target of 10,000 ions and a maximum injection time of 40 ms. Quantitative analysis of TMT-tagged peptides was performed using FTMS3 acquisition in the Orbitrap mass analyser operated at 60,000 resolution, with an AGC target of 100,000 ions and maximum injection time of 120 ms. Higher-energy C-trap dissociation (HCD fragmentation) on MS/MS fragments was performed in one-step collision energy of 55% to ensure maximal TMT reporter ion yield and synchronous-precursor-selection (SPS) was enabled to include 10 MS/MS fragment ions in the FTMS3 scan.

Protein identification and quantification were performed using MaxQuant version 1.5.1.759 with the following parameters: stable modification carbamidomethyl (C); variable modifications oxidation (M), acetylation (protein N terminus), deamidation (NQ), hydroxyproline (P), quantitation labels with 6plex TMT on N-terminal or lysine with a reporter mass tolerance of 0.01 Da and trypsin as enzyme with 2 missed cleavages. Search was conducted using a combined FASTA database of *Serratia marcescens* Db11 and the *Candida albicans* SC5314 (assembly 22) database61 (downloaded from www.candidagenome.org on September 1st 2015), including common contaminants. Mass accuracy was set to 4.5 ppm for precursor ions and 0.5 Da for ion trap MS/MS data. Identifications were filtered at a 1% FDR at the protein and peptide level, accepting a minimum peptide length of 7 amino acids. Quantification of identified proteins referred to razor and unique peptides, and required a minimum ratio count of 2. Normalized ratios were extracted for each protein/conditions and were used for downstream analyses.

Europe PMC Funders Author Manuscripts

Mass spectrometry data analysis

Data was further analysed using the Perseus software package62. Pairwise comparisons were made using unpaired Student's T-tests ($p<0.05$, two-sided). Multiple samples were analysed using ANOVA at $p<0.05$ (multiple sample test). Perseus was also used for heatmaps and clustering (Euclidean, 10 clusters) of ANOVA positive proteins. For the *S. marcescens* cellular proteome, proteins were identified as differentially abundant when at least two unique peptides were identified, intensities were detected in a minimum of two out of the six biological replicates, and average LFQ intensities were altered more than 1.4-fold ($|\log2| > 0.5$, p-value < 0.05). For the bacterially-intoxicated *C. albicans* proteome, modulated proteins had significant ANOVA score (p-value < 0.05) and strong effector-specific changes were identified by pairwise comparison (fold change >1.3, p-value < 0.05). Gene Ontology (GO) term analysis was carried out using the GO Term Finder Tool applying standard settings available at Candida Genome Database (CGD)63 (http://www.candidagenome.org/). This version of GO Term Finder uses a hypergeometric distribution with Multiple Hypothesis Correction to calculate p-values.

Supplementary Material

Refer to Web version on PubMed Central for supplementary material.

Acknowledgements

This work was supported by the Wellcome Trust (Senior Research Fellowship in Basic Biomedical Science to S.J.C., 104556; 097377, J.Q.; 101873 & 200208, N.A.R.G.), the MRC (MR/K000111X/1, S.J.C; MC_UU_12016/5, M.T.), and the BBSRC (BB/K016393/1 & BB/P020119/1, J.Q.). We thank Maximilian Fritsch, Mario López Martín and Birte Hollmann for help with strain construction; Gary Eitzen for construction of pGED1; Donna MacCallum for the gift of *Candida glabrata* ATCC2001; Joachim Morschhäuser for the gift of pNIM1; Gillian Milne (Microscopy and Histology facility, University of Aberdeen) for assistance with TEM; and Peter Taylor, Giuseppina Mariano, Michael Porter, Laura Monlezun and Colin Rickman for advice and technical assistance.

References

1. Boer W, Folman LB, Summerbell RC, Boddy L. Living in a fungal world: impact of fungi on soil bacterial niche development. FEMS Microbiol Rev. 2005; 29:795–811. [PubMed: 16102603]
2. Peleg AY, Hogan DA, Mylonakis E. Medically important bacterial-fungal interactions. Nat Rev Microbiol. 2010; 8:340–349. [PubMed: 20348933]
3. Costa TR, et al. Secretion systems in Gram-negative bacteria: structural and mechanistic insights. Nat Rev Microbiol. 2015; 13:343–359. [PubMed: 25978706]
4. Basler M. Type VI secretion system: secretion by a contractile nanomachine. Philos Trans R Soc Lond B Biol Sci. 2015; 370
5. Cianfanelli FR, Monlezun L, Coulthurst SJ. Aim, Load, Fire: The Type VI Secretion System, a Bacterial Nanoweapon. Trends Microbiol. 2016; 24:51–62. [PubMed: 26549582]
6. Durand E, Cambillau C, Cascales E, Journet L. VgrG, Tae, Tle, and beyond: the versatile arsenal of Type VI secretion effectors. Trends Microbiol. 2014; 22:498–507. [PubMed: 25042941]
7. Hachani A, Wood TE, Filloux A. Type VI secretion and anti-host effectors. Curr Opin Microbiol. 2016; 29:81–93. [PubMed: 26722980]
8. Alcoforado Diniz J, Liu YC, Coulthurst SJ. Molecular weaponry: diverse effectors delivered by the Type VI secretion system. Cell Microbiol. 2015; 17:1742–1751. [PubMed: 26432982]
9. Russell AB, Peterson SB, Mougous JD. Type VI secretion system effectors: poisons with a purpose. Nat Rev Microbiol. 2014; 12:137–148. [PubMed: 24384601]

10. Murdoch SL, et al. The opportunistic pathogen *Serratia marcescens* utilizes type VI secretion to target bacterial competitors. J Bacteriol. 2011; 193:6057–6069. [PubMed: 21890705]
11. Klis FM, de Koster CG, Brul S. Cell wall-related bionumbers and bioestimates of *Saccharomyces cerevisiae* and *Candida albicans*. Eukaryot Cell. 2014; 13:2–9. [PubMed: 24243791]
12. Fritsch MJ, et al. Proteomic identification of novel secreted antibacterial toxins of the *Serratia marcescens* type VI secretion system. Mol Cell Proteomics. 2013; 12:2735–2749. [PubMed: 23842002]
13. Peters BM, Jabra-Rizk MA, O'May GA, Costerton JW, Shirtliff ME. Polymicrobial interactions: impact on pathogenesis and human disease. Clin Microbiol Rev. 2012; 25:193–213. [PubMed: 22232376]
14. Turner SA, Butler G. The *Candida* pathogenic species complex. Cold Spring Harb Perspect Med. 2014; 4 a019778.
15. Cianfanelli FR, et al. VgrG and PAAR Proteins Define Distinct Versions of a Functional Type VI Secretion System. PLoS Pathog. 2016; 12:e1005735. [PubMed: 27352036]
16. English G, et al. New secreted toxins and immunity proteins encoded within the Type VI secretion system gene cluster of *Serratia marcescens*. Mol Microbiol. 2012; 86:921–936. [PubMed: 22957938]
17. Park YN, Morschhauser J. Tetracycline-inducible gene expression and gene deletion in *Candida albicans*. Eukaryot Cell. 2005; 4:1328–1342. [PubMed: 16087738]
18. Millard PJ, Roth BL, Thi HP, Yue ST, Haugland RP. Development of the FUN-1 family of fluorescent probes for vacuole labeling and viability testing of yeasts. Appl Environ Microbiol. 1997; 63:2897–2905. [PubMed: 9212436]
19. Essary BD, Marshall PA. Assessment of FUN-1 vital dye staining: Yeast with a block in the vacuolar sorting pathway have impaired ability to form CIVS when stained with FUN-1 fluorescent dye. J Microbiol Methods. 2009; 78:208–212. [PubMed: 19501122]
20. Hogan DA, Kolter R. *Pseudomonas-Candida* interactions: an ecological role for virulence factors. Science. 2002; 296:2229–2232. [PubMed: 12077418]
21. Braun BR, Johnson AD. Control of filament formation in *Candida albicans* by the transcriptional repressor TUP1. Science. 1997; 277:105–109. [PubMed: 9204892]
22. Marzluf GA. Molecular genetics of sulfur assimilation in filamentous fungi and yeast. Annu Rev Microbiol. 1997; 51:73–96. [PubMed: 9343344]
23. Kraidlova L, et al. Characterization of the Candida albicans Amino Acid Permease Family: Gap2 Is the Only General Amino Acid Permease and Gap4 Is an S-Adenosylmethionine (SAM) Transporter Required for SAM-Induced Morphogenesis. mSphere. 2016; 1
24. Sychrova H, Souciet JL. CAN1, a gene encoding a permease for basic amino acids in *Candida albicans*. Yeast. 1994; 10:1647–1651. [PubMed: 7725800]
25. Matijekova A, Sychrova H. Biogenesis of *Candida albicans* Can1 permease expressed in *Saccharomyces cerevisiae*. FEBS Lett. 1997; 408:89–93. [PubMed: 9180275]
26. Ljungdahl PO, Daignan-Fornier B. Regulation of amino acid, nucleotide, and phosphate metabolism in *Saccharomyces cerevisiae*. Genetics. 2012; 190:885–929. [PubMed: 22419079]
27. Ljungdahl PO. Amino-acid-induced signalling via the SPS-sensing pathway in yeast. Biochem Soc Trans. 2009; 37:242–247. [PubMed: 19143640]
28. Brega E, Zufferey R, Mamoun CB. *Candida albicans* Csy1p is a nutrient sensor important for activation of amino acid uptake and hyphal morphogenesis. Eukaryot Cell. 2004; 3:135–143. [PubMed: 14871944]
29. Didion T, Regenberg B, Jorgensen MU, Kielland-Brandt MC, Andersen HA. The permease homologue Ssy1p controls the expression of amino acid and peptide transporter genes in *Saccharomyces cerevisiae*. Mol Microbiol. 1998; 27:643–650. [PubMed: 9489675]
30. Iraqui I, et al. Amino acid signaling in *Saccharomyces cerevisiae*: a permease-like sensor of external amino acids and F-Box protein Grr1p are required for transcriptional induction of the AGP1 gene, which encodes a broad-specificity amino acid permease. Mol Cell Biol. 1999; 19:989–1001. [PubMed: 9891035]

31. Klasson H, Fink GR, Ljungdahl PO. Ssy1p and Ptr3p are plasma membrane components of a yeast system that senses extracellular amino acids. Mol Cell Biol. 1999; 19:5405–5416. [PubMed: 10409731]
32. Tripathi G, et al. Gcn4 co-ordinates morphogenetic and metabolic responses to amino acid starvation in *Candida albicans*. EMBO J. 2002; 21:5448–5456. [PubMed: 12374745]
33. Hinnebusch AG. Mechanisms of gene regulation in the general control of amino acid biosynthesis in *Saccharomyces cerevisiae*. Microbiol Rev. 1988; 52:248–273. [PubMed: 3045517]
34. Reggiori F, Klionsky DJ. Autophagic processes in yeast: mechanism, machinery and regulation. Genetics. 2013; 194:341–361. [PubMed: 23733851]
35. Guan J, et al. Cvt18/Gsa12 is required for cytoplasm-to-vacuole transport, pexophagy, and autophagy in *Saccharomyces cerevisiae* and *Pichia pastoris*. Mol Biol Cell. 2001; 12:3821–3838. [PubMed: 11739783]
36. Delorme-Axford E, Guimaraes RS, Reggiori F, Klionsky DJ. The yeast *Saccharomyces cerevisiae*: an overview of methods to study autophagy progression. Methods. 2015; 75:3–12. [PubMed: 25526918]
37. Cebollero E, Reggiori F. Regulation of autophagy in yeast *Saccharomyces cerevisiae*. Biochim Biophys Acta. 2009; 1793:1413–1421. [PubMed: 19344676]
38. Rubin-Bejerano I, Fraser I, Grisafi P, Fink GR. Phagocytosis by neutrophils induces an amino acid deprivation response in *Saccharomyces cerevisiae* and *Candida albicans*. Proc Natl Acad Sci U S A. 2003; 100:11007–11012. [PubMed: 12958213]
39. Fradin C, et al. Granulocytes govern the transcriptional response, morphology and proliferation of *Candida albicans* in human blood. Mol Microbiol. 2005; 56:397–415. [PubMed: 15813733]
40. Lorenz MC, Bender JA, Fink GR. Transcriptional response of *Candida albicans* upon internalization by macrophages. Eukaryot Cell. 2004; 3:1076–1087. [PubMed: 15470236]
41. Jimenez-Lopez C, et al. *Candida albicans* induces arginine biosynthetic genes in response to host-derived reactive oxygen species. Eukaryot Cell. 2013; 12:91–100. [PubMed: 23143683]
42. Basler M, Pilhofer M, Henderson GP, Jensen GJ, Mekalanos JJ. Type VI secretion requires a dynamic contractile phage tail-like structure. Nature. 2012; 483:182–186. [PubMed: 22367545]
43. Dupres V, Dufrene YF, Heinisch JJ. Measuring cell wall thickness in living yeast cells using single molecular rulers. ACS Nano. 2010; 4:5498–5504. [PubMed: 20804167]
44. Yamaguchi M, et al. Structome of *Saccharomyces cerevisiae* determined by freeze-substitution and serial ultrathin-sectioning electron microscopy. J Electron Microsc (Tokyo). 2011; 60:321–335. [PubMed: 21908548]
45. Hoarau G, et al. Bacteriome and Mycobiome Interactions Underscore Microbial Dysbiosis in Familial Crohn's Disease. MBio. 2016; 7
46. Mahlen SD. *Serratia* infections: from military experiments to current practice. Clin Microbiol Rev. 2011; 24:755–791. [PubMed: 21976608]
47. Haapalainen M, et al. Hcp2, a secreted protein of the phytopathogen *Pseudomonas syringae* pv. tomato DC3000, is required for fitness for competition against bacteria and yeasts. J Bacteriol. 2012; 194:4810–4822. [PubMed: 22753062]
48. Amberg DC, Burke D, Strathern JN, Burke D. Cold Spring Harbor Laboratory. Methods in Yeast Genetics: a Cold Spring Harbor Laboratory course manual. Edn. 2005. Cold Spring Harbor Laboratory Press; New York: 2005.
49. Allan C, et al. OMERO: flexible, model-driven data management for experimental biology. Nat Methods. 2012; 9:245–253. [PubMed: 22373911]
50. Schindelin J, et al. Fiji: an open-source platform for biological-image analysis. Nat Methods. 2012; 9:676–682. [PubMed: 22743772]
51. te Winkel JD, Gray DA, Seistrup KH, Hamoen LW, Strahl H. Analysis of Antimicrobial-Triggered Membrane Depolarization Using Voltage Sensitive Dyes. Front Cell Dev Biol. 2016; 4
52. Knop M, et al. Epitope tagging of yeast genes using a PCR-based strategy: more tags and improved practical routines. Yeast. 1999; 15:963–972. [PubMed: 10407276]
53. Miller-Fleming L, Cheong H, Antas P, Klionsky DJ. Detection of *Saccharomyces cerevisiae* Atg13 by western blot. Autophagy. 2014; 10:514–517. [PubMed: 24430166]

54. Kurz CL, et al. Virulence factors of the human opportunistic pathogen *Serratia marcescens* identified by *in vivo* screening. EMBO J. 2003; 22:1451–1460. [PubMed: 12660152]
55. Petty NK, Foulds IJ, Pradel E, Ewbank JJ, Salmond GP. A generalized transducing phage (phiIF3) for the genomically sequenced *Serratia marcescens* strain Db11: a tool for functional genomics of an opportunistic human pathogen. Microbiology. 2006; 152:1701–1708. [PubMed: 16735733]
56. Naujoks J, et al. IFNs Modify the Proteome of Legionella-Containing Vacuoles and Restrict Infection Via IRG1-Derived Itaconic Acid. PLoS Pathog. 2016; 12:e1005408. [PubMed: 26829557]
57. Guo M, et al. High-resolution quantitative proteome analysis reveals substantial differences between phagosomes of RAW 264.7 and bone marrow derived macrophages. Proteomics. 2015; 15:3169–3174. [PubMed: 25504905]
58. Dill BD, et al. Quantitative proteome analysis of temporally resolved phagosomes following uptake via key phagocytic receptors. Mol Cell Proteomics. 2015; 14:1334–1349. [PubMed: 25755298]
59. Cox J, Mann M. MaxQuant enables high peptide identification rates, individualized p.p.b.-range mass accuracies and proteome-wide protein quantification. Nat Biotechnol. 2008; 26:1367–1372. [PubMed: 19029910]
60. Ritorto MS, Cook K, Tyagi K, Pedrioli PG, Trost M. Hydrophilic strong anion exchange (hSAX) chromatography for highly orthogonal peptide separation of complex proteomes. J Proteome Res. 2013; 12:2449–2457. [PubMed: 23294059]
61. Muzzey D, Schwartz K, Weissman JS, Sherlock G. Assembly of a phased diploid *Candida albicans* genome facilitates allele-specific measurements and provides a simple model for repeat and indel structure. Genome Biol. 2013; 14:R97. [PubMed: 24025428]
62. Tyanova S, et al. The Perseus computational platform for comprehensive analysis of (prote)omics data. Nat Methods. 2016; 13:731–740. [PubMed: 27348712]
63. Skrzypek MS, et al. The Candida Genome Database (CGD): incorporation of Assembly 22, systematic identifiers and visualization of high throughput sequencing data. Nucleic Acids Res. 2017; 45:D592–D596. [PubMed: 27738138]
64. Vizcaino JA, et al. 2016 update of the PRIDE database and its related tools. Nucleic Acids Res. 2016; 44:D447–456. [PubMed: 26527722]

Europe PMC Funders Author Manuscripts

Europe PMC Funders Author Manuscripts

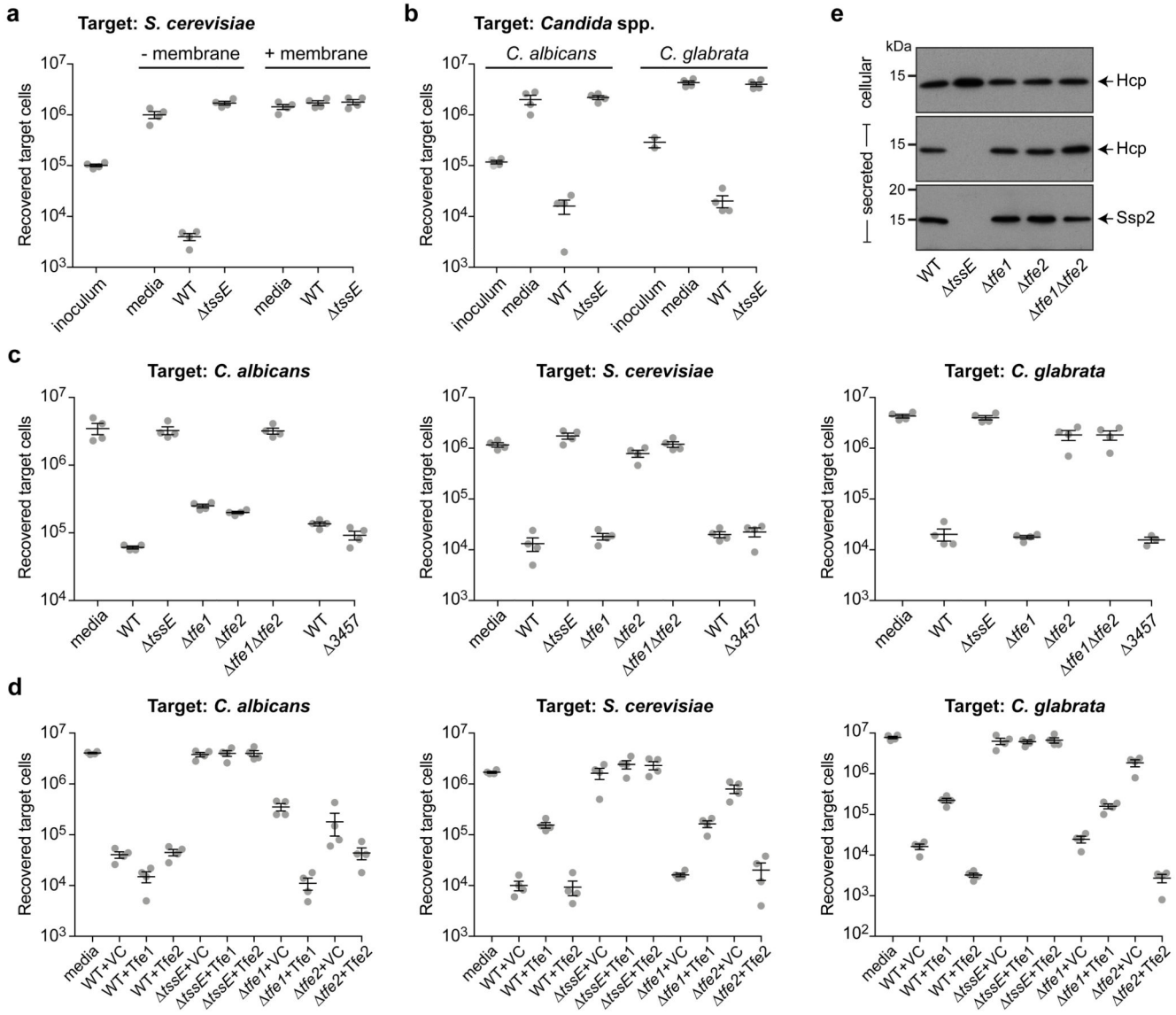

Figure 1. Cross-kingdom targeting by the Type VI secretion system of *S. marcescens* depends on the anti-fungal effectors Tfe1 and Tfe2.

(a) Number of recovered viable cells of *S. cerevisiae* K699 following co-culture with wild type (WT) or a T6SS-inactive mutant (Δ*tssE*) strain of *S. marcescens* Db10 as attacker, or with sterile media alone (media), in the absence or presence of a separating membrane. (b) Recovery of *C. albicans* SC5314 and *C. glabrata* ATCC2001 following co-culture with wild type or a T6SS-inactive mutant of *S. marcescens*. (c) Recovery of *C. albicans*, left, *S. cerevisiae*, middle, and *C. glabrata*, right, following co-culture with wild type or mutant (Δ*tssE*, Δ*tfe1*, Δ*tfe2*, Δ*tfe1*Δ*tfe2* and Δ*SMDB11_3457*) *S. marcescens*. (d) Recovery of *C. albicans*, *S. cerevisiae* and *C. glabrata* following co-culture with wild type or mutant strains of *S. marcescens* Db10 carrying either the vector control plasmid (+VC, pSUPROM), or a plasmid directing the expression of Tfe1 with the immunity protein Sip3 (+Tfe1), or Tfe2 (+Tfe2). (e) Immunoblot detection of Hcp1 and Ssp2 in cellular and secreted fractions of

wild type or mutant *S. marcescens* as indicated. The data are representative of two independent experiments and the full, uncropped blots can be found in Supplementary Fig. 18. In parts a-d, individual data points are overlaid with the mean +/- SEM (n=4 biological replicates).

Europe PMC Funders Author Manuscripts

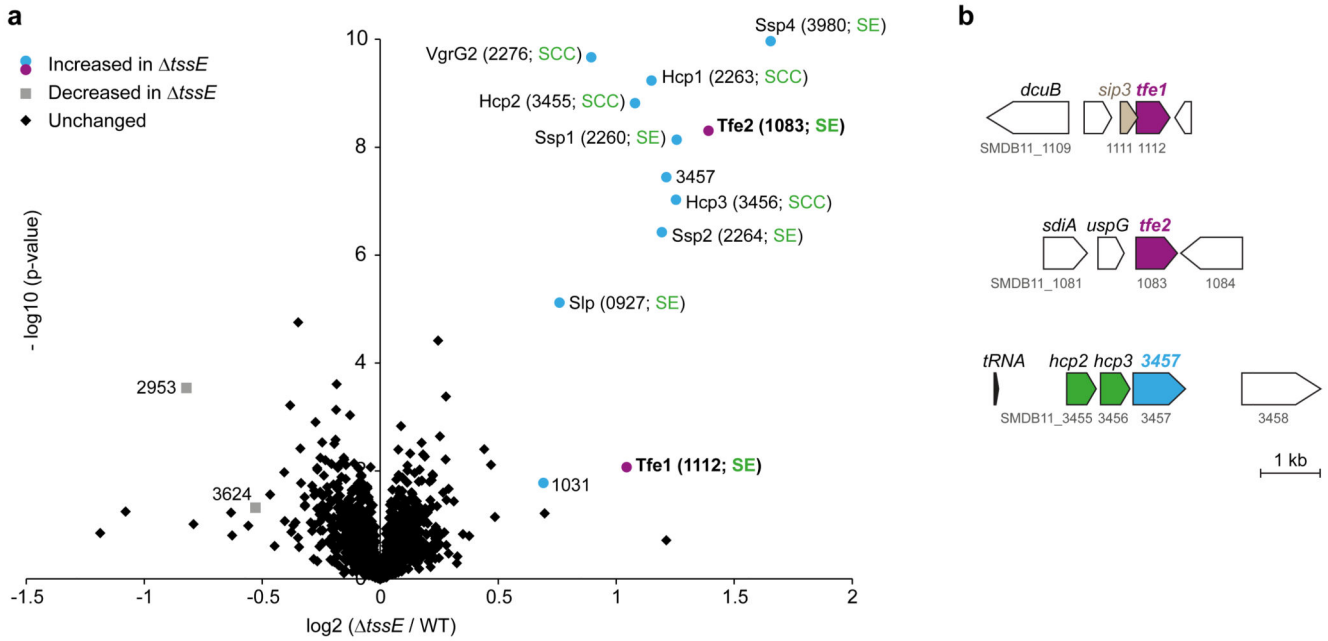

Figure 2. Quantitative cellular proteomics identifies known and previously-unidentified T6SS-secreted proteins.

(a) Volcano plot summarising the proteomic comparison of total intracellular proteins between the wild type (WT) and a T6SS-inactive mutant (Δ*tssE*) strain of *S. marcescens* Db10 using label-free quantitation. The log2 of the ratios of protein intensities between the wild type and the Δ*tssE* mutant are plotted against the –log10 of t-test p-values (unpaired t-test, two-sided; n=6 biological replicates). Proteins significantly increased in abundance in the Δ*tssE* mutant compared with the wild type (Δ*tssE*/WT > 1.4-fold, $p < 0.05$) are depicted as circles, with magenta circles representing those secreted effectors (SE) identified as anti-fungal effectors in this study, and blue circles representing other hits, including secreted core components (SCC) or previously identified secreted effectors. Grey squares represent proteins significantly decreased in abundance in the Δ*tssE* mutant compared with the wild type (Δ*tssE*/WT < -1.4-fold, $p < 0.05$) and black diamonds correspond to proteins without significant changes. Numbers in brackets represent genomic identifiers for the proteins (SMDB11_xxxx). (b) Schematic depiction of the genetic loci containing the *tfe1*, *tfe2* and *SMDB11_3457* genes in *S. marcescens* Db10. The *sip3* gene encodes the previously identified immunity protein for Tfe1/Ssp3.

Europe PMC Funders Author Manuscripts

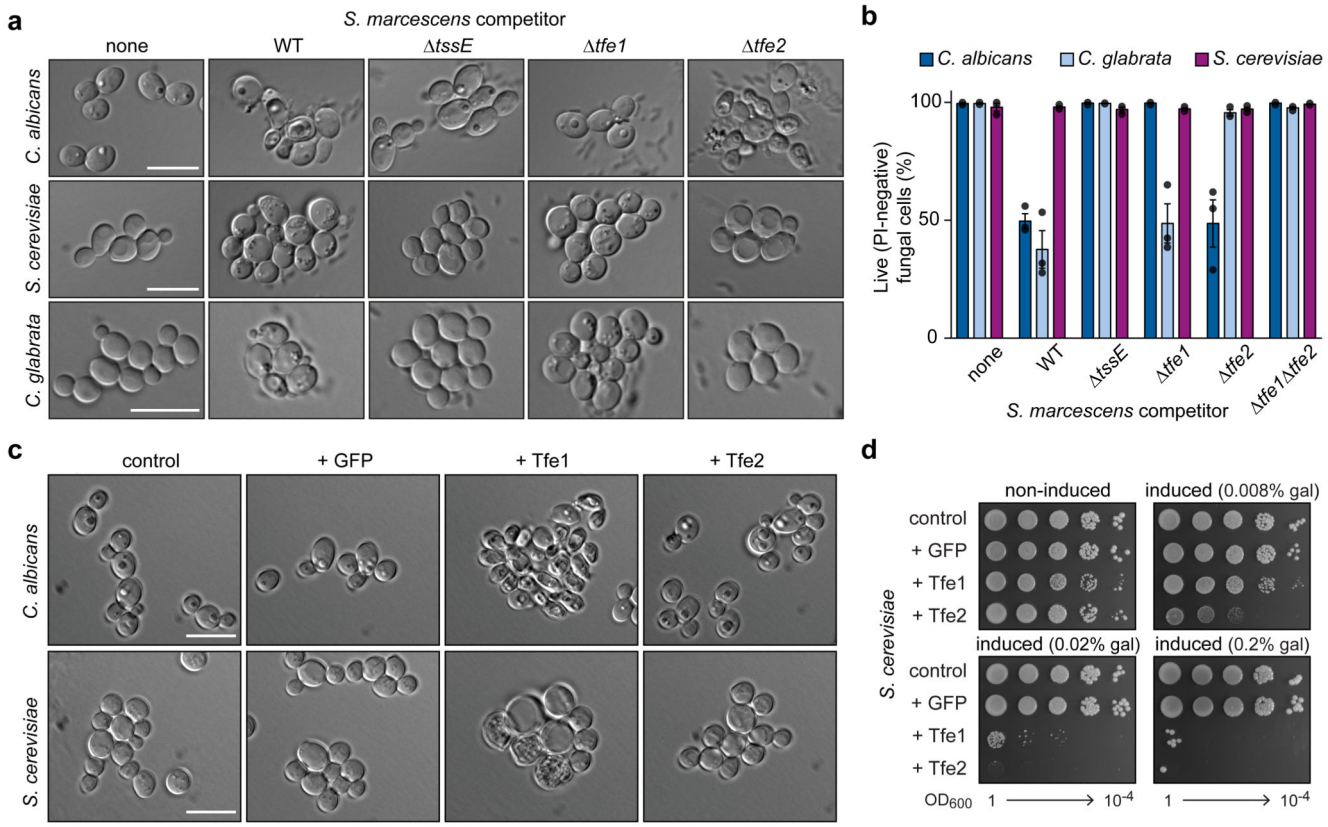

Figure 3. Tfe1 and Tfe2 are anti-fungal toxins that impact fungal cell integrity.

(a) DIC microscopy of target strains *C. albicans* SC5314, *S. cerevisiae* K699 and *C. glabrata* ATCC2001, following co-culture with wild type or mutant (Δ*tssE*, Δ*tfe1*, Δ*tfe2*, Δ*tfe1*Δ*tfe2*) strains of *S. marcescens* Db10. 'None' indicates co-culture of the target with media alone. Representative of three independent experiments. (b) Percentage of live fungal cells of *C. albicans*, *C. glabrata* and *S. cerevisiae*, following co-culture with strains of *S. marcescens*, as indicated by propidium iodide (PI) staining. Bars show mean +/- SEM (n=3 independent experiments, with individual data points shown). (c) DIC microscopy of *C. albicans* SC5314 (control) and derivatives expressing GFP, Tfe1 or Tfe2, upper panel, and *S. cerevisiae* K699 carrying the control plasmid pRB1438 or GFP-, Tfe1- or Tfe2-expression plasmids, lower panel. Representative of two independent experiments. (d) Growth of *S. cerevisiae* K699 chromosomal integration strains harbouring the empty promoter construct (control) or constructs for expression of GFP, Tfe1 or Tfe2, on non-inducing and inducing media (gal, galactose). Representative of two independent experiments. In parts a and c, scale bars represent 10 μm and scale is the same across each row of images.

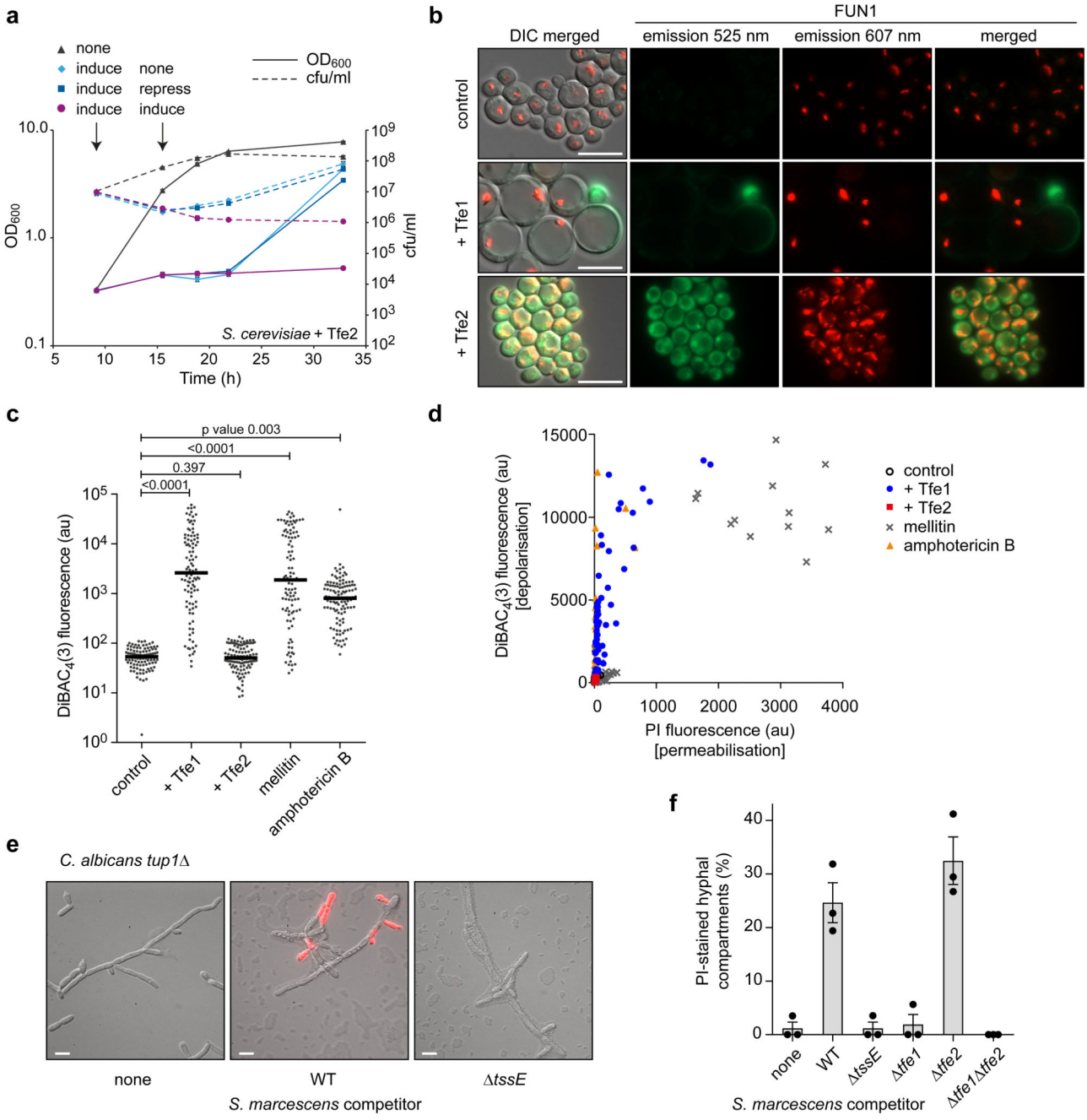

Figure 4. T6SS-mediated effector delivery disrupts fungal metabolic activity and membrane potential, and can act against hyphal cells.

(a) Growth of *S. cerevisiae* expressing Tfe2 as determined by cell density (OD_{600}) and viable cell counts (cfu/ml). Time-course presented includes an induction period in non-inducing (none, 2% raffinose) or inducing media (induce, 2% raffinose 2% galactose), followed by either relief (none, 2% raffinose), repression (repress, 2% raffinose 2% glucose) or ongoing (induce, 2% raffinose 2% galactose) expression of Tfe2. Points show mean +/- SEM (n=3). (b) Fluorescence microscopy of FUN1-stained *S. cerevisiae* cells expressing GFP, Tfe1 or Tfe2. The single and merged green and red fluorescence channels, and their

overlays on the corresponding DIC image are shown. Representative of two independent experiments. (c) Quantification of fluorescence from *S. cerevisiae* cells expressing Tfe1 or Tfe2, following staining with the potential-sensitive dye $DiBAC_4(3)$. Control cells were additionally treated with 10 μM mellitin (membrane depolarization through pore formation) or 3 μg/ml amphotericin B (membrane depolarization without pore formation). Points represent individual cells and bars show mean (p values are indicated; unpaired, two-sided t-test; n=100-116). (d) Quantification of cellular $DiBAC_4(3)$ and propidium iodide (PI) fluorescence for cells expressing Tfe1 or Tfe2, or treated with mellitin or amphotericin B. Scatter plots depict fluorescence intensity values of individual cells for both dyes (au, arbitary units; n=95-128). Example microscopy images and separate scatter plots are in Supplementary Fig. 8. (a)-(d) *S. cerevisiae* strains were K699 chromosomal integration strains harbouring the empty promoter construct (control) or constructs for galactose-inducible expression of GFP, Tfe1 or Tfe2. (e) Representative images and (f) quantification of PI staining of hyphae of the constitutively filamentous *tup1*Δ mutant of *C. albicans*, following co-culture with the strains of *S. marcescens* Db10 indicated (none, media only; WT, wild type). Bars show mean +/- SEM (n=3 independent experiments, individual data points shown), images are representative of four independent experiments. In parts b and e, scale bars represent 10 μm.

Europe PMC Funders Author Manuscripts

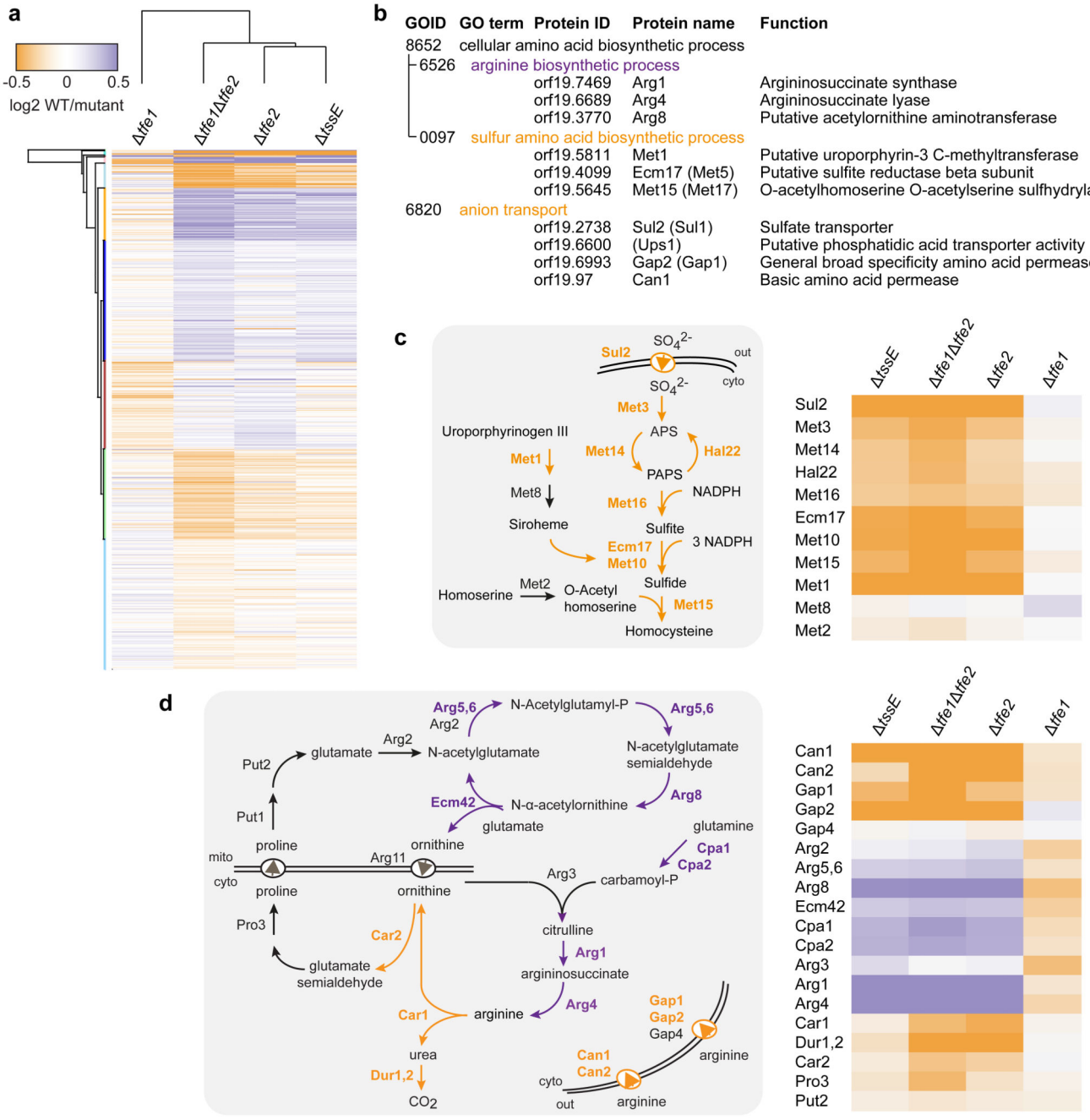

Figure 5. 'In competition' quantitative proteomics reveals interference of Tfe2 with fungal nutrient uptake and metabolism.

(a) Heat map showing hierarchical clustering of the differential proteome of *C. albicans* SC5314 following co-culture with wild type *S. marcescens* Db10 compared with mutant (Δ*tssE*, Δ*tfe1*, Δ*tfe2* and Δ*tfe1*Δ*tfe2*) strains of Db10. All 1667 proteins with significant ANOVA scores ($p<0.05$, n=6 biological replicates) are included and the full cluster analysis with gene identifiers is available as Supplementary Data 4. (b) GO terms significantly enriched ($p<0.05$) in the set of 30 *C. albicans* SC5314 proteins identified as significantly responsive to Tfe2 (Supplementary Table 1). Where different, the protein name in *S.*

Europe PMC Funders Author Manuscripts

cerevisiae is given in brackets. (c,d) Schematic illustration (left panels) and corresponding heat-maps of the pathway-associated proteins (right panels) of the sulfate assimilation and arginine biosynthesis pathways in fungal cells. Proteins increased in abundance following co-culture with wild type *S. marcescens* as compared with the mutant strains indicated are shown in purple, and proteins decreased are shown in orange.

Europe PMC Funders Author Manuscripts

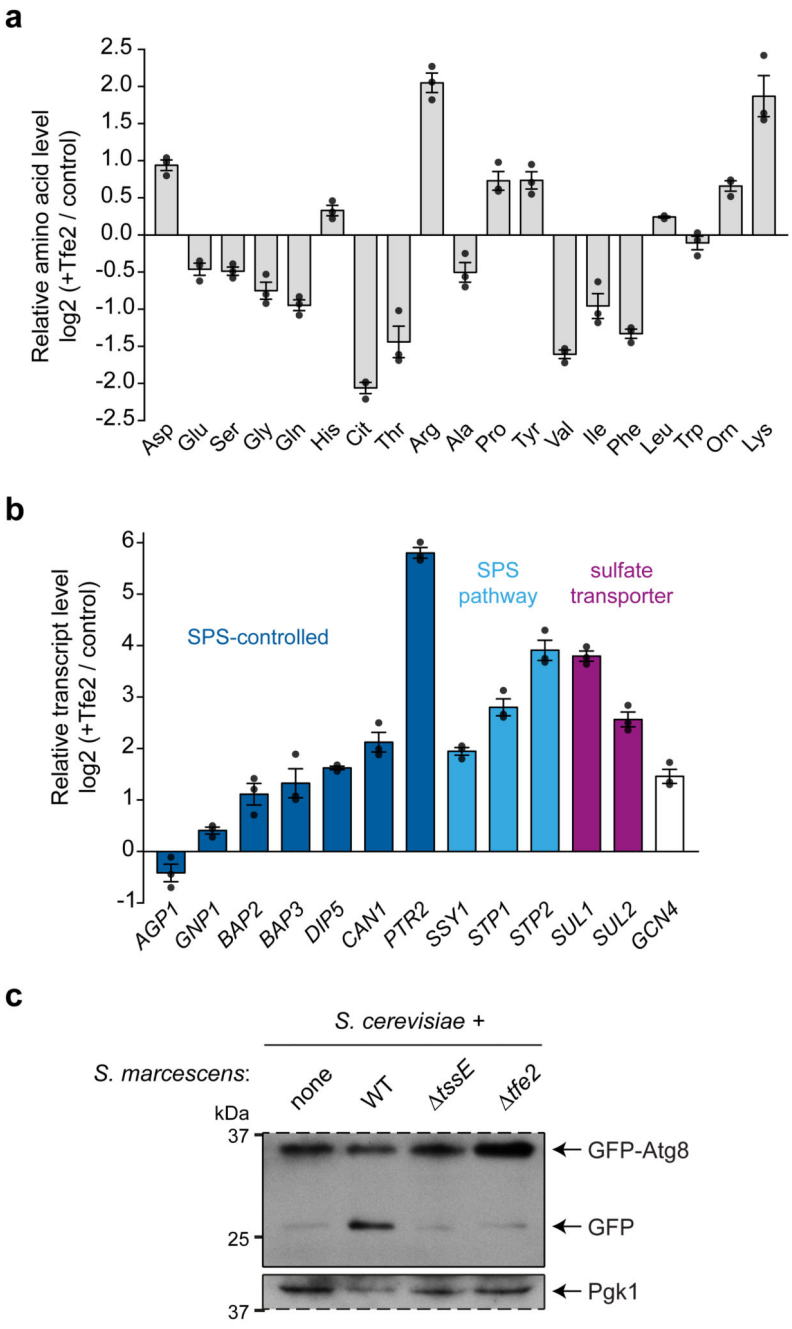

Figure 6. Tfe2 alters the cellular amino acid pool and induces autophagy in fungal cells.

(a) Relative levels of total intracellular amino acids in *S. cerevisiae* K699 expressing plasmid-borne Tfe2 (+Tfe2) compared with the vector control (Cit, citrulline; Orn, ornithine). Bars show log2 of the mean +/- SEM (n=3 biological replicates), with individual data points shown. (b) Differential expression analysis of genes involved in nutrient sensing and starvation in *S. cerevisiae* expressing Tfe2 relative to the vector control. qRT-PCR analysis was performed on transcripts of genes for amino acid permease and dipeptide transporters that are under the control of the amino acid sensor complex SPS (*AGP1*, *GNP1*,

Europe PMC Funders Author Manuscripts

BAP2, *BAP3*, *DIP5, CAN1, PTR2*), the SPS sensor component (*SSY1*), the SPS-activated transcriptional regulators (*STP1*, *STP2*), the sulfate transporter (*SUL1*, *SUL2*) and the general amino acid control response regulator (*GCN4*). Bars show log2 of the mean relative transcript abundance +/- SEM (n=3 biological replicates). (c) Immunoblot detection of GFP-Atg8 processing in *S. cerevisiae* K699 following co-culture with wild type (WT) or mutant (Δ*tssE* and Δ*tfe2*) strains of *S. marcescens* Db10 using anti-GFP antibody. Yeast cells carry the reporter plasmid GFP-ATG8(416) directing expression of GFP-Atg8 from the endogenous Atg8 promoter. GFP-Atg8 has a MW of 41 kDa and cleaved GFP is 27 kDa. Pgk1 was used as control cellular protein and dashed line indicates where the blot membrane was cut to allow detection with the two different antibodies; the full, uncropped blots can be found in Supplementary Fig. 18. These data are representative of three independent experiments.